International Journal of Ocean Engineering and Technology Vol. 4, No. 1, pp 22~30, April 2001 (ISSN 1229-1668)

# A Study on Numerical Modeling of a Wave Absorber

WON MIN MOON*, SUN HONG KWON* AND HEE SUNG LEE*

*Dept. of Naval Architecture & Ocean Engineering, Pusan National University, Pusan, Korea*
*(Received 30 January 2001, accepted 19 March 2001)*

**ABSTRACT:** *A new concept wave absorber is proposed. It is a net type wave absorber. Its efficiency was reported in another publication. Since it is based on new concept, the traditional wave absorber theory is not applicable. It is modeled by introducing damping terms in linearized free surface boundary conditions in this study. The length and the thickness of the wave absorber are modeled by the length and the coefficient of the damping terms. Series of experiments are carried out to get the data for the coefficients of the damping term. The boundary element method is adopted to solve the system. The predicted wave heights show excellent agreement with those of experiments when the lengths of the incoming waves are within the length of the wave absorber.*

**KEY WORDS:** Net-Type Wave Absorber, Numerical Modeling, Artificial Damping Method, Boundary Element Method, Linearized Freesurface Boundary Conditions.

## 1. Introduction

To avoid wave reflection from the end of wave tank or side wall, every wave tank has wave absorbing devices. The simplest one is wave absorbing beach and elaborate one is active wave absorber. Similar to the real wave tank, Numerical Wave Tank (NWT)s have wave absorbing function. Wave absorbing method used in NWTs can be classified into three categories, (1) application of Sommerfield radiation condition, (2) physical wave absorbing method used in real wave tank and (3) artificial wave absorbing method. In this study, artificial damping method is adopted to design efficient wave absorber which is applicable in small wave flume. Artificial wave absorbing methods are called as sponge layer, artificial beach or damping zone. In this paper, these methods are generally referred as damping zone. In damping zone, artificial damping terms are added to free surface boundary conditions. In the former research(Lee, 2000), we invented net-type wave absorber, which works so well in small wave flume. In this paper numerical modeling started with the idea that there must be some relationships between numerical damping zone and real net-type wave absorber(Mooon, 2001). The Length of the real wave absorber is characterized with that of artificial damping zone. The thickness of the net-type wave absorber is correlated with strength of damping term,, damping coefficient The boundary element methad was adopted to rolve the oystem(Kim, 1994), (Boo, 1993). To validate these numerical modeling, an experiment is performed in various length and thickness of net- type wave absorber. Comparison among numerical and experimental results shows that artificial damping zone can be a good simulator to predict the behavior of net-type wave absorber.

## 2. Mathematical Formulation

Fig. 1 shows a 2D fluid domain bounded by free surface, flap type wave maker, bottom and wall of wave flume. The space fixed coordinate x-z is used to figure out 2D domain. In the coordinate system, z is positive upward and z=0 coincides with calm water surface. The hinge of the flap type wave maker is located at the x=0 position.

There are two artificial damping zones to describe the performance of net-type wave absorbers as shown in Fig. 2. The first one is to see how efficiently the wave absorber works, the second is just to suppress the waves which is not absorbed by the first absorber, and it prevents the numerical errors, which is due to the reflected waves from the other side of wave flume.

The fluid is assumed to be homogeneous, incompressible and its motion irrotational. The fluid motion can be described by a velocity potential $\phi$. Due to the assumptions made, the function $\phi$ satisfies the Laplace equation,

$$\nabla^2\phi(x,z,t)=0, \text{ in } \Omega \tag{1}$$

On the free-surface, linear kinematic boundary condition and dynamic boundary condition are applied and damping terms are added to them to give artificial damping effects to free-surface. The free-surface boundary conditions inside a damping zone are given as

$$\frac{\partial\phi}{\partial t}+g\eta+\nu(x)=0 \tag{2}$$

$$\frac{\partial \phi}{\partial n} = \frac{\partial \eta}{\partial t} + \nu(x)\eta \tag{3}$$

where $\nu(x)$ is the damping coefficient (4)

$$\nu_1(x) = \alpha_1 \omega \frac{x - x_{d1}}{L_{d1}} \tanh\left[\frac{\pi(x - x_{d1})}{L_{d1}}\right], \tag{4}$$

for $x_{d1} \le x \le x_{d1} + L_{d1}$

$$\nu_2(x) = \alpha_2 \omega \frac{x - x_{d2}}{L_{d2}} \tanh\left[\frac{\pi(x - x_{d2})}{L_{d2}}\right], \tag{5}$$

for $x_{d2} \le x$

$\nu_1(x) = \nu_2(x) = 0$,

for otherwise (6)

where $\nu_1(x)$ is to describe the net-type wave absorber which is located at the center of wave flume, while $\nu_2(x)$ is to satisfy the radiation condition of the NWT, and it is located at the end of wave flume. In the equations of $\nu_1(x)$ and $\nu_2(x)$, $\omega$ and $L_d$ are angular frequency and the length of the artificial damping zone, respectively. $x_{d1}$, $x_{d2}$ represent the front and end position of the wave absorber in $x$ axis. The characteristic of these damping zones is controlled by two parameter $\alpha$ and $L_d$. $\alpha$ is used to control the strength of damping zone and $L_d$ is to control the length of damping zone. In other words, each of them describes the characteristics thickness and length- of net-type wave absorber. The length of the real net-type wave absorber is characterized with that of artificial damping zone.

For flap type wave maker, boundary condition is applied on the mean position of it,

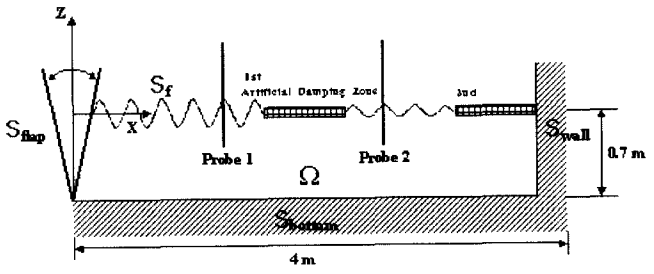


**Fig. 1** Numerical Domain

**Fig. 2** Experimental Domain

$$u(0,z,t) = \frac{\omega}{2} S(z)\cos\omega t \quad \text{at} \quad x=0$$

# 3. Numerical Implementation

## 3.1 Discrete Formulation

The new equation is derived from the boundary integral equation, which is as follows.

$$c^i \phi^i + \sum_{j=1}^{n} \hat{H}_{ij}\phi_j = \sum_{j=1}^{n} G_{ij} \frac{\partial \phi_j}{\partial n} \tag{7}$$

Considering all the boundary conditions along the domain of the consideration - free surface $\Gamma_f$, wave maker $\Gamma_{flap}$, bottom $\Gamma_b$ and the end of wave flume $\Gamma_{wall}$, Eq. (7) can be written for the $n+m$ elements. The free surface is divided into $n$ straight line segments while other boundaries are divided into $m$ segments.

$$c^i \phi^i + \sum_{j=1}^{m+n} \hat{H}_{ij}\phi_j - \sum_{j=1}^{n} G_{ij} \frac{\partial \phi_j}{\partial n} - \sum_{j=n+1}^{n(\Gamma_{flap})} G_{ij}\left[\frac{S_j}{2}\omega\cos\omega t\right] = 0 \tag{8}$$

In Eq. (8), the third term can be replaced by the following kinematic free surface boundary condition.

$$\frac{\partial \phi_j}{\partial n} = \frac{\partial \eta_j}{\partial t} + \nu_j \eta_j$$

Substituting the kinematic free surface boundary condition, the normal derivative term of the velocity potential is eliminated. It causes problems at the intersection point between two boundaries, which have different boundary conditions.

$$c^i \phi^i + \sum_{j=1}^{m+n} \hat{H}_{ij}\phi_j - \sum_{j=1}^{n} G_{ij}\left[\frac{\partial \eta_j}{\partial t} + \nu_j \eta_j\right] - \sum_{j=n+1}^{n(\Gamma_{flap})} G_{ij}\left[\frac{S_j}{2}\omega\cos\omega t\right] = 0 \tag{9}$$

Linearized dynamic free surface boundary condition can be written as follows

$$\frac{\partial \phi_j}{\partial t} + g\eta_j + \nu_j \phi_j = 0 \tag{10}$$

## 3.2 Time Integration of Boundary Conditions

To discretize $\phi$ and $\eta$ with respect to time, time is divided into $\Delta t$, $t_k \le t \le t_{k+1} (= t_k + \Delta t)$

$$\dot{\phi}(t) = \frac{\dot{\phi}^{k+1} - \dot{\phi}^{k}}{\Delta t}(t - t_k) + \dot{\phi}^{k} \tag{11}$$

where superscription k represents time index.

Integrate Eq. (11) with respect to time, $t$

$$\phi(t)=\frac{\dot{\phi}^{k+1}-\dot{\phi}^{k}}{2\Delta t}(t-t_k)^2+\dot{\phi}^{k}(t-t_k)+\phi^{k} \tag{12}$$

Let $t=t_{k+1}$

$$\phi^{k+1}=\phi^{k}+\frac{\Delta t}{2}(\dot{\phi}^{k+1}+\dot{\phi}^{k}) \tag{13}$$

Eq. (13) can be written as

$$\dot{\phi}^{k+1}=\frac{2}{\Delta t}(\phi^{k+1}-\phi^{k})-\dot{\phi}^{k} \tag{14}$$

$\eta$ can be derived in the same way as the above

$$\dot{\eta}^{k+1}=\frac{2}{\Delta t}(\eta^{k+1}-\eta^{k})-\eta^{k} \tag{15}$$

Consider Eq. (9) and (10) as the equation at the time of $t_{k+1}$ substitute Eq. (14) and (15) into Eq. (9) and (10)

$$c_i\phi_i^{k+1}+\sum_{j=1}^{m+n}\hat{H}_{ij}\phi_j^{k+1}-\sum_{j=1}^{n}G_{ij}\left[\frac{2}{\Delta t}(\eta_j^{k+1}-\eta_j^{k})-\dot{\eta}_j^{k}+\nu_j\eta_j^{k}\right] \tag{16}$$

$$-\sum_{j=n+1}^{n(\Gamma_{flap})}G_{ij}\left[\frac{S_j}{2}\omega\cos\omega t\right]=0 \quad (i=1,2,\ldots,n)$$

$$\frac{2}{\Delta t}(\phi_j^{k+1}-\phi_j^{k})-\dot{\phi}_j^{k}+\nu_j\phi_j^{k+1}+g\eta_j^{k+1}=0 \tag{17}$$

$$(j=1,2,\ldots,m)$$

The last discretized integral equations are

$$c_i\phi_i^{k+1}+\sum_{j=1}^{m+n}\hat{H}_{ij}\phi_j^{k+1}-\frac{2}{\Delta t}\sum_{j=1}^{n}G_{ij}\eta_j^{k+1}$$

$$=\sum_{j=1}^{n}G_{ij}\left[\left(\frac{2}{\Delta t}+\nu_j\right)\eta_j^{k}-\dot{\phi}_j^{k}\right]+\sum_{j=n+1}^{n(\Gamma_{flap})}G_{ij}\left[\frac{S_j}{2}\omega\cos\omega t\right] \tag{18}$$

$$(i=1,2,\ldots,n)$$

$$\left(\frac{2}{\Delta t}+\nu_j\right)\phi_j^{k+1}+g\eta_j^{k+1}=\frac{2}{\Delta t}\phi_j^{k}+\dot{\phi}_j^{k} \tag{19}$$

$$(j=1,2,\ldots,m)$$

In Eq. (18) and (19), the unknowns are the velocity potential $\phi^{k+1}$ on the all boundaries and wave elevation $\eta^{k+1}$ on the free surface. The method of time integration used in this section, leads us without using the normal derivative of velocity potential. Therefore, the problem in dealing with the normal velocity at the intersection node between two segments becomes easier(Nakayama, 1981).

## 4. Experimental Setup

The wave flume used for the experimental studies is illustrated in figure 2. Waves are generated by a flap type wave maker, travel from left to right, and are normally absorbed by a net-type wave absorber. The side walls and base of the tank are glass, allowing good optical access. The flume is 4m long and 0.3m wide. The water depth is 0.7m.

The net-type wave absorber was invented as shown in Fig. 3a with the requirements that the length of the flume is so short that the wave is reflected from the other side and the need of powerful wave absorber was critical. Many other useful type of wave absorber was inefficient for the small wave flume. We

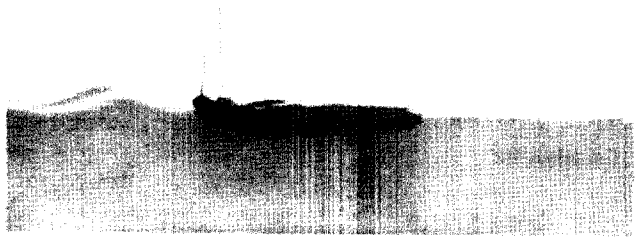

**Fig. 3a** Net-type Wave Absorber

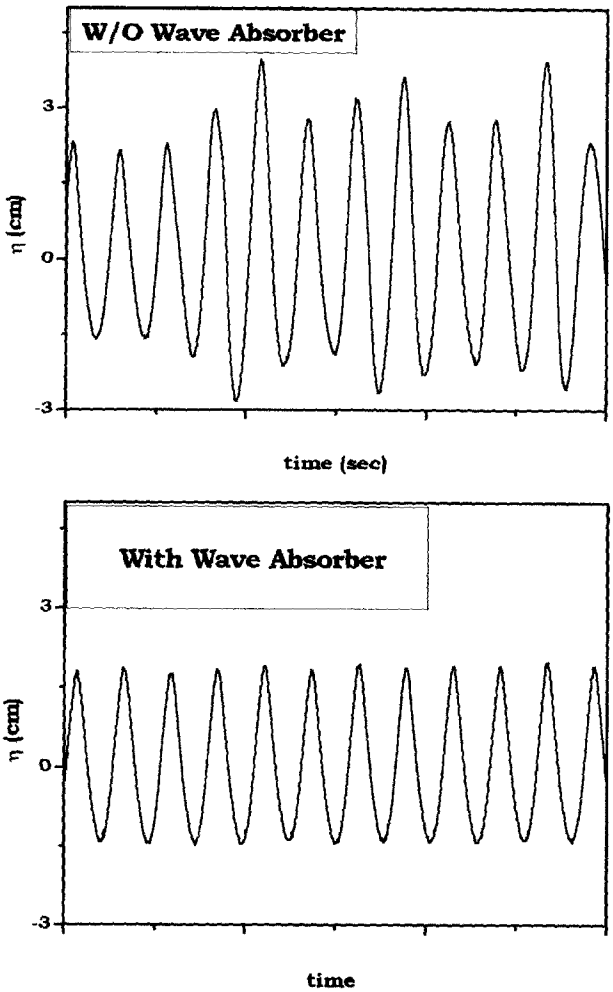


**Fig. 3b** Time history of wave elevation without and with wave absorber

designed new type one with the idea that flexibe and dense net layer will suppress the wave through its dense holes.[3] The size of net hole is about 0.5mm, to carry out a systematical experiment we designed unit net-1A , by folding it five times from 1.8m×1.6m to 0.3m×0.4m.

The time history of wave elevation with/without wave absorber are shown in Fig. 3b, respectively. It vividly shows the efficiency of net-type wave absorber.

Table 1 shows the dimension of net-type wave absorber. We carried out forteen cases of experiement with varing the length and the thickness of the flexible dense net layer.

A flap type wave maker is hinged at the bottom; and move fowards and backwards via a drive arm which is in line with the torque motor and transforms the rotating motion to direct one. The frequency and stroke of the wave are cotrolled by the rpm of motor and radius of rotating motion, respectively.

The gauges used to measure wave height in the studies were wire wave gauges of the conductive type. Digital camorder and video capturing systems are also used to generate movie files. The locations of probes were 5 cm apart from the front and 5 cm apart from the rear end of the wave absorber.

## 5. Experimental Results

Both in the experiment and numerical simulation, the wave length and incident wave height were 40cm and 3cm, respectively. As described in the above, the net-type wave absorbers are sited both on the center and the end of the wave flume. The original purpose of the wave absorber is certainly to suppress(prevent) the wave from reflecting to the other side. But the reason why a wave absorber is laid on the center of the wave flume is to observe how efficiently it works and also to measure the wave height in front of and behind it. The wave height, measured both in front of damping zone(H) and behind of it(h) and the ratio of them is defined as the damping ratio(h/H).

First of all, six sets of experiments are carried out to measure the efficiency of a wave absorber. Each set has different thickness of net-type wave absorber but the same length. The thickness are changed from 1A to 7A, while the length are 40cm which is same as the incident wave length. The experimental time histories of wave height in front of and behind wave absorber are shown in Fig. 14 to Fig. 17. The solid line is the wave height measured by the first wave gauge which is in front of net-type absorber and the broken line is measured by the second probe which is located behind the wave absorber. From the results of each experiment, the absorbing ratio(h/H) with respect to the thickness of wave absorber is calculated. Fig. 21 shows that the absorbing ratio with respect to the thickness of wave absorber. Obviously, as thickness gets bigger, the net-type wave absorber works more efficiently. When the thickness of absorber is 10A, the incident wave is suppressed at the rate of 78%. The incident wave height is reduced from 1.5cm to 0.27cm. Although the incidents waves are suppressed efficiently according to the thickness of the wave absorber, there are some diffraction problems in front of excessively thick one.

**Table 1** Experimental cases1

| case no. | unit no. | number of fold | Length×width×thickness |
|---|---|---|---|
| case1 | 1A | 1 | 0.4m×0.3m×5mm |
| case2 | 2A | 2 | 0.4m×0.3m×10mm |
| case3 | 3A | 3 | 0.4m×0.3m×15mm |
| case4 | 4A | 4 | 0.4m×0.3m×20mm |
| case5 | 5A | 5 | 0.4m×0.3m×25mm |
| case6 | 6A | 6 | 0.4m×0.3m×30mm |
| case7 | 7A | 7 | 0.4m×0.3m×35mm |

Secondly, in order to make a proper simulation , damping coefficient $\alpha_1$ in Eq.. (4) which gives the corresponding absorbing ratio on each case of experiments with different thickness, is numerically determined as shown in Fig. 20. The damping coefficient of artificial damping zone, $\alpha_1$ is from 0.1 to 0.51 corresponding to the thickness of wave absorber from 1A to 10A. The numerical time histories of wave height in front of and behind the artificial damping zone are shown in Fig. 7 to Fig. 10. During above two steps, the lengths of real wave absorber and artificial damping zone are fixed to 40 cm length. Therefore, the effect of the length of wave absorber is not considered.

Thirdly, using the damping coefficient $\alpha_1$ determined for each thickness of wave absorber in the previous steps, the length of damping zone is enlarged from 40cm to 70cm while the thickness is 5A and the coefficient $\alpha_1$ is 0.25. The time histories of wave height with respect to the length of real-net type wave absorber are shown in Fig. 11(t=5A, Ld=40cm) to Fig. 13.(t=5A, Ld=70cm). As the wave absorber is longer, the incident waves are suppressed more efficiently. In order to use the numerical simulation as a method for predicting the efficiency of wave absorber , it must give the same results not only for different thickness of wave absorber but also for different length. The time histories for each case in which the length of artificial damping zone is changed from 40cm to 70cm, while the strength of damping coefficient is fixed to 0.25, are shown in Fig. 4 to Fig. 6. The absorbing ratio of artificial damping zone with respect to the length of damping zone is summarized in Fig. 18. Comparing with the results from experiments, it can be seen that there are big similarity between them. The gradient between damping

efficiency and the length of damping zone is 4.03 for the experiment and it is 4.08 for the simulation. In the case of 40cm of wave absorber, first, the damping coefficient is chosen numerically, and next using this value, numerical simulation is carried out with various length of wave absorber, without any further experiment. It is due to the values of each gradient, -4.03 and 4.08 are not much different.

Now let's change the subject to the usefulness of the numerical model. In order to validate the usefulness of the numerical simulation, predictions for the cases of different length and different thickness of wave absorber are performed. Several points connected with solid lines in Fig. 22 shows the results of numerical prediction.

First, the strength of the damping coefficient for 40cm length of artificial damping zone is numerically determined to give the same absorbing efficiency with respect to the thickness of real net-type wave absorber.

Second, the absorbing efficiency is numerically calculated for each thickness of wave absorber.-i.e. for each strength of damping coefficient. The length is enlarged from 40cm to 70cm. Each connected solid line indicates the damping ratio by numerical prediction. In order to confirm the validation of numerical results, six different cases of net-type wave absorber are made and the experiments for each case are carried out. Solid circles 1A,2A,3A,5A,7A and 10A denote them. As shown in Fig. 22, absorbing efficiencies predicted by numerical simulation reach good agreement with them determined by the experiments for the length of 50cm .

But there are slight differences between them in the case of 60cm. The reason for some differences between numerical and experimental results can be explained as follows. Firstly, as the real net-type wave absorber gets longer, it makes its own motion due to the flexibility of the floating net-type wave absorber. As the results of the motion of wave absorber, some waves suddenly happen which can not be predicted in numerical modeling. Secondly, it could not work well without some contradiction in the view of wave kinematics to keep the strength of damping coefficient constant along the damping zone. It might be impossible to consider all the performance of floating net-type wave absorber without simplifications and assumptions. The numerical modeling which describes the performance of net-type wave absorber is developed. In conclusion, it seems to be reasonable to replace the thickness of wave absorber to the strength coefficient of artificial damping zone. The length of the absorbing device is directly related with that of damping zone. The results of numerical prediction and the experimental

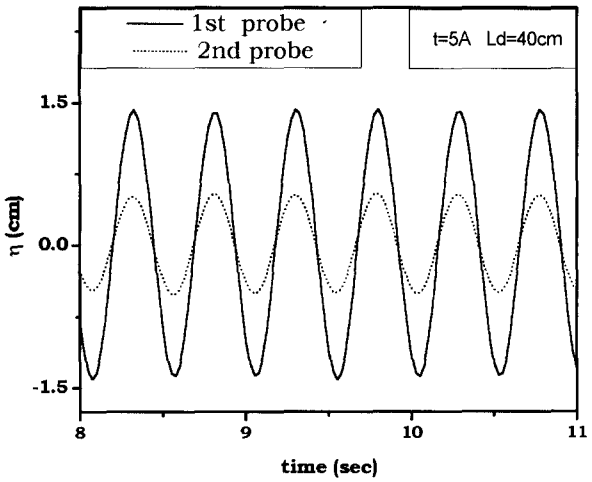


**Fig. 4** Numerical time history (α=0.25,Ld=40cm)

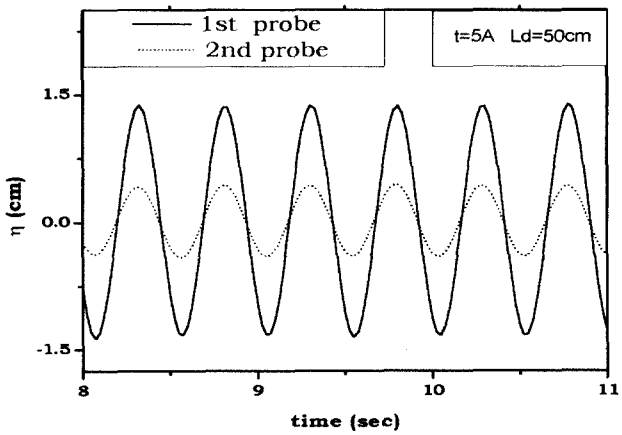


**Fig. 5** Numerical time history (=0.25,Ld=50cm)

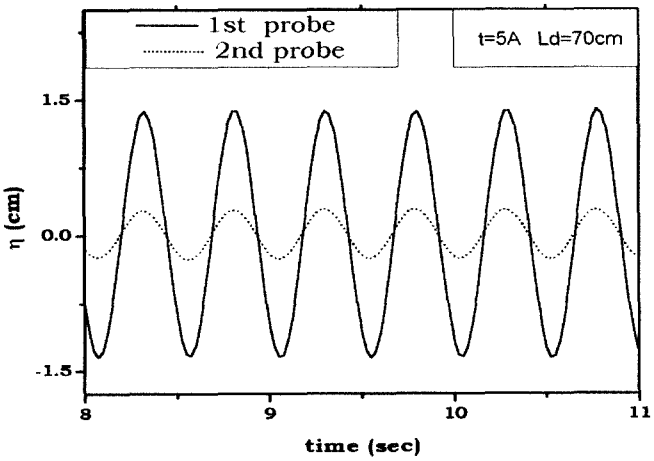


**Fig. 6** Numerical time history (=0.25,Ld=70cm)

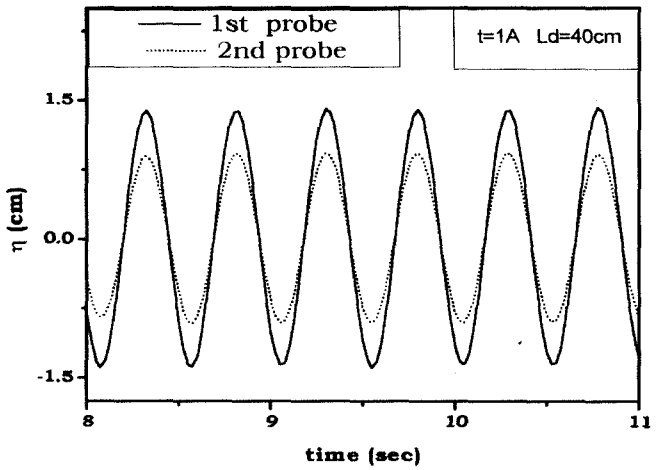


Fig. 7 Numerical time history (t=1A,Ld=40cm)

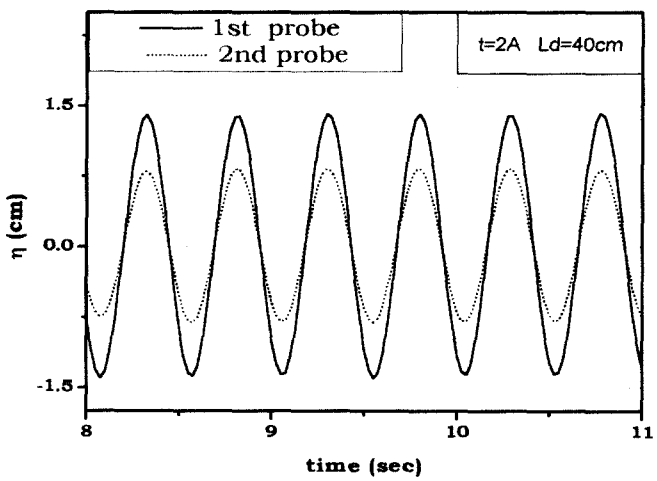


Fig. 8 Numerical time history (t=2A,Ld=40cm)

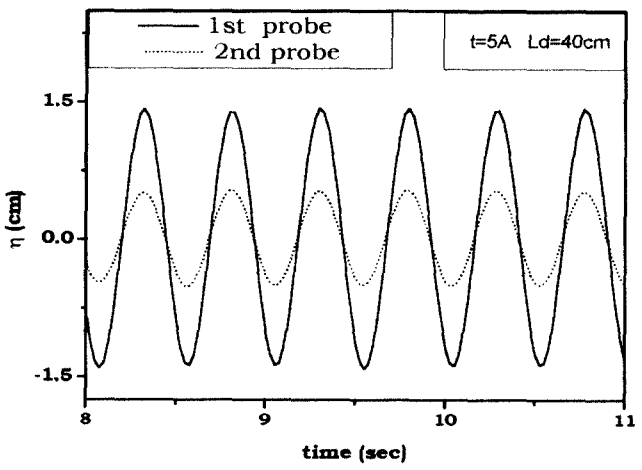


Fig. 9 Numerical time history (t=5A,Ld=40cm)

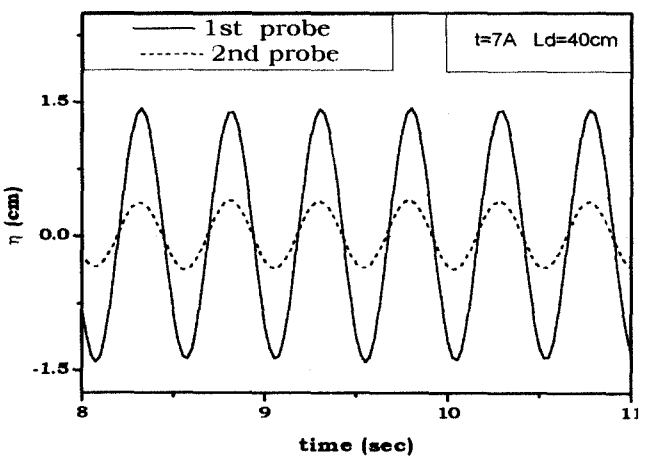


Fig. 10 Numerical time history (t=7A,Ld=40cm)

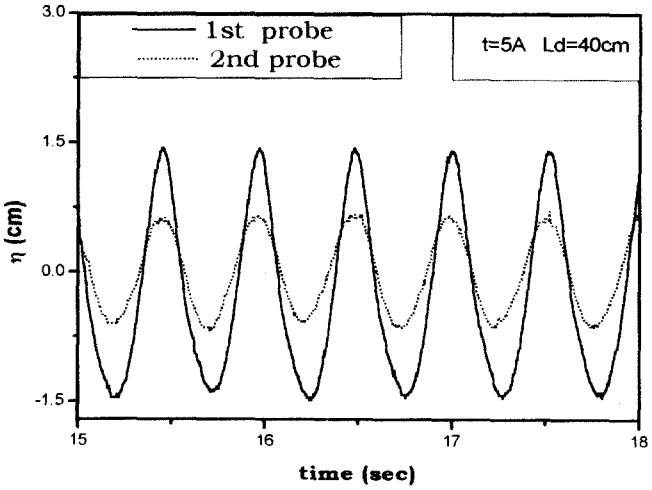


Fig. 11 Experimental time history (t=5A,Ld=40cm)

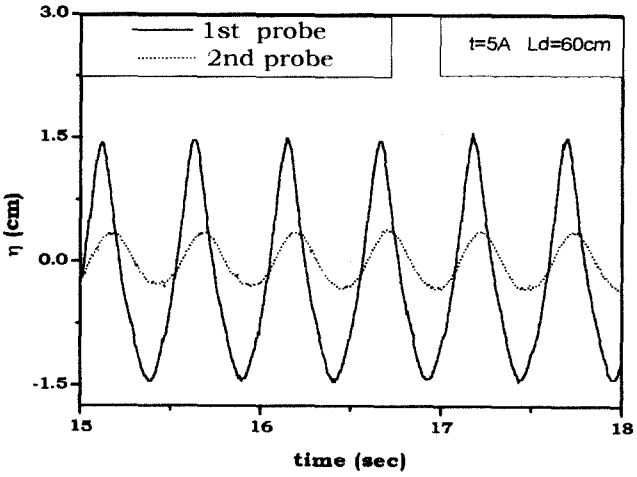


Fig. 12 Experimental time history (t=5A,Ld=60cm)

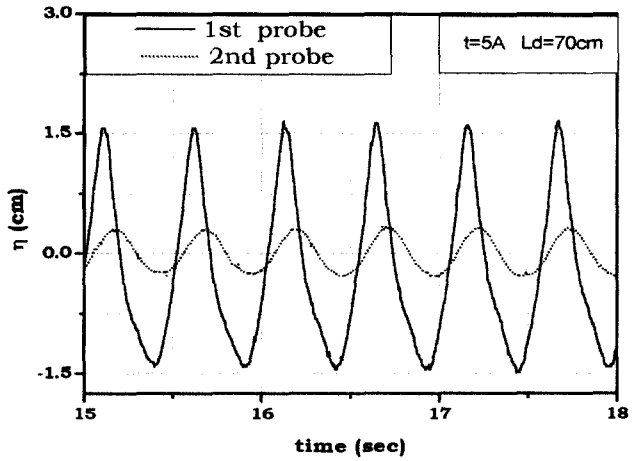


Fig. 13 Experimental time history (t=5A,Ld=70cm)

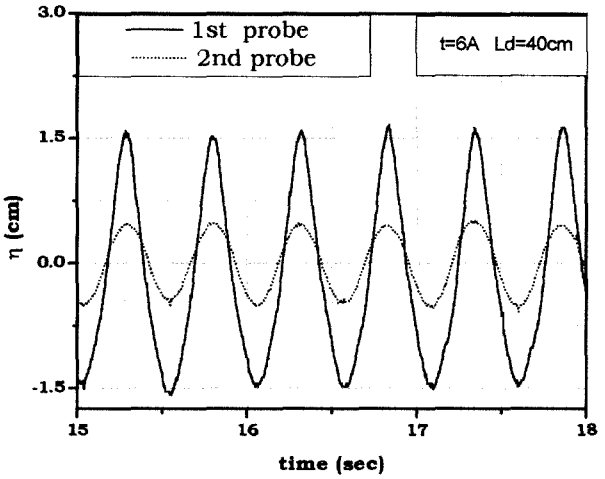


Fig. 16 Experimental time history (t=6A,Ld=40cm)

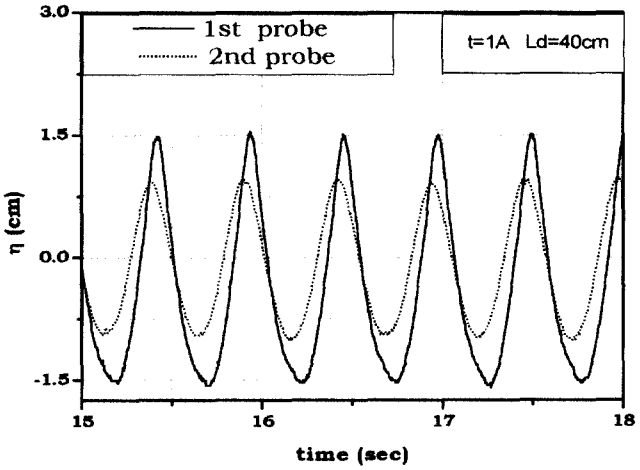


Fig. 14 Experimental time history (t=1A,Ld=40cm)

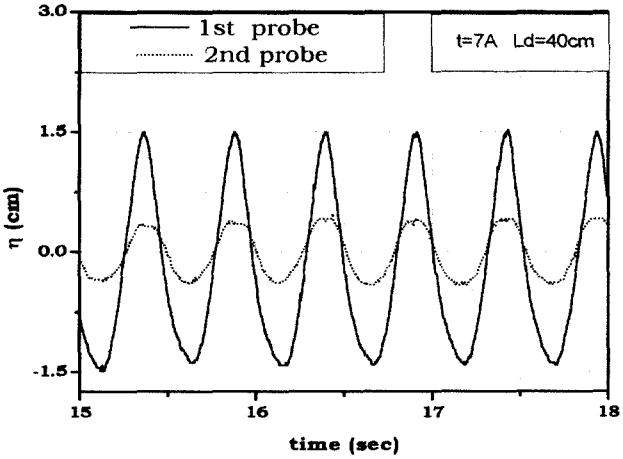


Fig. 17 Experimental time history (t=7A,Ld=40cm)

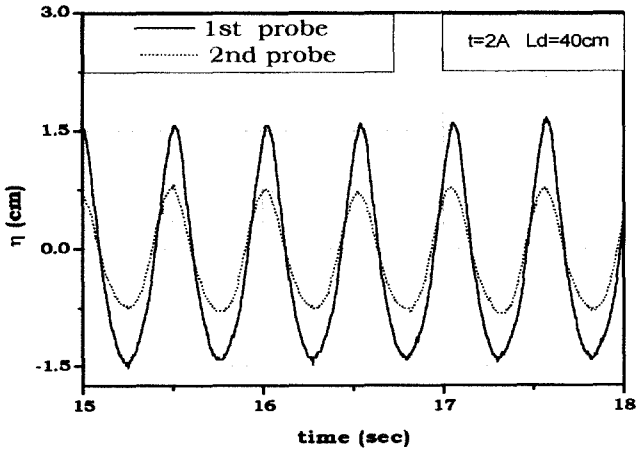


Fig. 15 Experimental time history (t=2A,Ld=40cm)

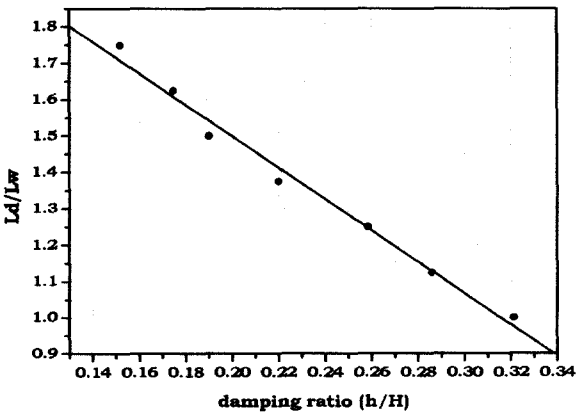


Fig. 18 Numerical damping ratio vs Length of damping zone

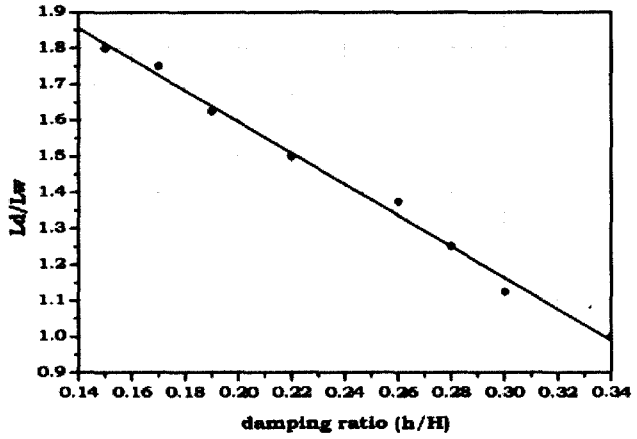


Fig. 19 Experimental damping ratio vs Length of wave absorber

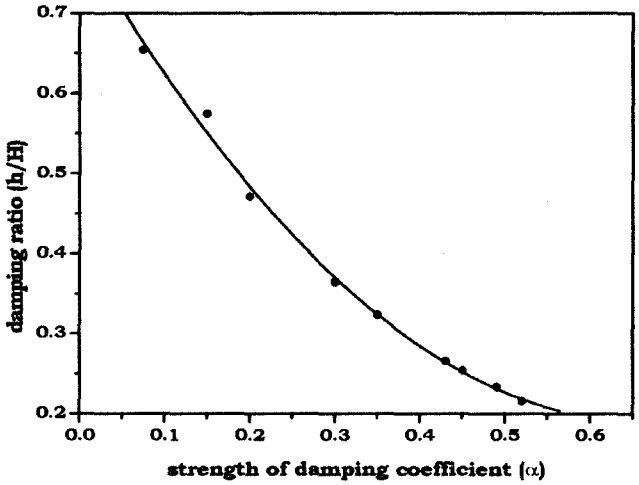


Fig. 20 Numerical damping ratio vs strength of damping coeff.

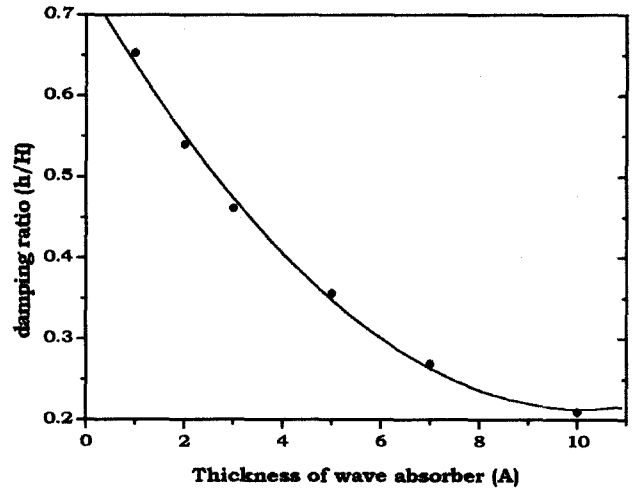


Fig. 21 Experimental damping ratio vs Thickness of wave absorber

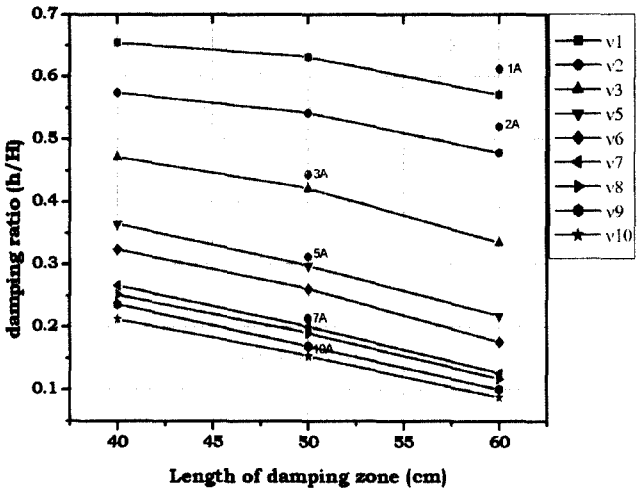


Fig. 22 Numerical prediction vs Experimental validation

validation, they have a good agreement.

Wave absorbing device is useful not only in wave basin but also has so many application in the field of ocean engineering. In the economic sense, it is very cheap. In the view of installation, also it has very wide feasibility. However, the efficiency of net-type wave absorber decreases quickly as the incident wave is longer than absorbing device. Therefore, the length of the net-type wave absorber must be longer than the incident wave.

## 6. Conclusion

In this study, numerical modeling was presented which is applicable to the design of the net-type wave absorber. In order to describe the wave absorber, artificial damping zone is added to the linearized free surface boundary condition and numerically implemented by boundary element method. The length and the strength of the artificial damping zone are used to characterize the length and the thickness of net-type wave absorber. From the experiment in which the length of wave absorber is 40cm, the strength of artificial damping zone is determined which gives the same absorbing efficiency, and using this value, expand the length of damping zone. As results, the numerical simulation agreed well with the experiments.

The following conclusions can be drawn from the present study,

1. The net-type wave absorber can be modeled as an artificial damping zone.
2. The thickness of the wave absorber can be modeled in terms of the strength of artificial damping zone.
3. The length of the wave absorber can be modeled by replacing the length of damping zone.
4. As long as the length of the wave is within the order of

the length of the wave absorber, the proposed numerical modeling shows excellent agreement with those of the experiment.

5. The proposed wave absorber is an excellent device in absorbing the incoming wave energy. Many applications can be made in the field of ocean engineering.

## References

(1) Lee, H.S., Kwon, S.H., Jo, H.J., "An Experimental Study on Development of the Wave Absorber for Small Wave Flume," Journal of the Society of Naval Architects of Korea, Vol. 38, No. 1, pp 37~42, 2000.

(2) Moon, W.M., Kwon, S.H., Lee, H.S., A Study on Numerical Modeling of Wave Absorber, Proceeding of the Annual Spring Meeting of the Society of Naval Architects of Korea, pp 105~109, 2001.

(3) Tanizawa. K., "The state of the art on the numerical wave tank," Proceeding of 4th Osaka Colloquium on Seakeeping Performance of Ships, pp 95~114, Osaka, Japan, 2000.

(4) Sung, H.G., Choi, H.S., "Numerical Analysis of two-dimensional nonlinear radiation problem using higher-order boundary element method," Proceeding of the annual autumn meeting, SNAK, pp 290~293, 1999.

(5) Kim, Y.H., "A Study on the treatment of open boundary in the two-dimensional free surface wave problems," Selected Papers of SNAK, Vol. 2. pp 63~78, 1994.

(6) Boo, S.Y., "Application of higher order boundary element method to steady ship wave problem and time domain simulation of nonlinear gravity waves," Ph.D. Dissertation, Texas A&M Univ. 1993.

(7) Nakayama, T., Washizu, K. "The Boundary Element Method applied to the Analysis of two-dimensional nonlinear sloshing problems", International Journal for Numerical Methods in Engineering, Vol. 17, pp 1631~1646, 1981.